Nigerian Journal of Applied Physics (NJAP)
ISSN Print: 3115-5871
ISSN Online: 3115-588X
DOI: https://doi.org/10.62292/njap-v2i2-2026-82
Volume 2(2), June 2026

Fabrication and Characterization of Tungsten and Bismuth Nano Structured Protective Shields against X-rays

***Terver Daniel, Sylvester J. Gemanam, Emanuel H. Agba and Mrumun D. Tyona**

Department of Physics, Rev. Fr. Moses Orshio Adasu University, Makurdi, Benue State, Nigeria.

*Corresponding author's email: tdaniel@bsum.edu.ng

ABSTRACT

Interest have been shown in finding novel, effective and highly safe radiation shielding materials to replace the commonly used radiation shielding materials like lead that are heavy, toxic and environmentally hazardous. In this study, W and Bi nano structured protective shields were fabricated and characterized for use against X-rays. WO_3 and Bi_2O_3 nano powders with particle size 0.4 µm were used and the PVC powder and DOP oil were used as softeners for shields. Two sets of sample shields made of tungsten and bismuth were formed with thicknesses 1.5, 2.0 and 2.5 ± 0.4 mm, respectively. The sample shields were exposed to X-rays with X-ray tube voltages of 40, 50, and 60 kVp, for all the thicknesses. The half value layers and the attenuation coefficients of the shielding materials at varying thicknesses were determined. At 40 and 50 kVp X-rays exposures, Bi indicate higher attenuation properties than W, whereas at 60 kVp, both protective shields showed similar effect. At 50 and 60 kVp X-rays exposures, Bi showed higher attenuation coefficients as compared to W for all the various thicknesses of the shield used. The findings showed that the nano-structured samples have attenuating abilities and that Bi attenuating ability at 60 kVp is closer to lead than W, this shows that these nano-structured materials have potentials to replace lead.

Keywords:
Radiation shields,
X-rays,
Half-value layer,
Aattenuation Coefficients.

INTRODUCTION

Medical radiological examinations are widely used for diverse diagnostic and treatment-planning purposes in clinical practice. Although excessive radiation exposure increases the health risks to the populace. X-rays, Computed Tomography (CT), and other high-dose procedures such as interventional fluoroscopy and nuclear medicine in Europe and the United States are considered responsible for 78-89% of the total annual radiation exposure from medical imaging (Power et al., 2016). X-rays accounted for up to 50 % of the patient's radiation exposure from all radiographic examinations. Hence, the need to identify appropriate shielding materials for radiation oncologists and patients during X-ray and CT examinations (Huda, 2007).

The radiation risk to tissues is related to the magnitude of the corresponding absorbed dose, which can be classified as either Deterministic effects, characterized by the induction of individual skin burns and epilation, being associated with a threshold dose or Stochastic effects, which does not have threshold dose for its occurrence (Agba, 2017).

Certain materials and metallic oxides can serve as attenuators or shields of radiation beam in form of polymer fillers or composites. In this context, some composite materials containing compounds or elements such as barium sulfate, copper, gadolinium, gold, lead, molybdenum, rhodium, silver, tungsten, bismuth, zirconium oxide, iron oxide, and zinc have been extensively studied (AbuAlRoos et al., 2020). At present, composites containing bismuth are widely used as protective shields in radiological CT scans. Recent researchers have demonstrated that nanoparticles of few metallic oxides can effectively shield staff and patients against ionizing radiation (AbuAlRoos et al., 2020). Bismuth oxides are considered an interesting material due to their dielectric properties and applications in optical coatings, metal-insulator-semiconductor capacitors, and microwave-integrated circuits. Tungsten was used because of its high density and high atomic number which can enhance its shielding properties.

The use of lead as a radiation shielding material has been applied in a variety of applications. This includes diagnostic imaging, radiation therapy, nuclear shielding, and industry. It is also one of the most used radiation shielding materials for X-rays and gamma radiation due to its high density, high atomic number, and high linear and mass attenuation coefficients. However, lead materials can cause harmful effects when ingested or inhaled directly or through lead-contaminated materials. Radiation workers sometimes bring lead waste into their homes via clothing, skin, hair, and work equipment after dealing with lead in their workplace. This necessitates researching for appropriate radiation shields to protect humans and the environment from the harmful effects of radiation. To minimize the deleterious effects of radiation exposure from lead materials, including lead shield aprons, there is an increasing interest in research for new attenuating materials that are free of lead but have a high atomic number. Tungsten (due to its high density) and bismuth (because of its atomic number, which is higher than that of lead) are the preferred materials of choice for investigation (Nikeghbal, et al., 2020).

Choosing a suitable type of radiation shield is primarily based on the cost, weight, chemical and physical resistance of the material. Herein, we investigate the radiation shielding efficiency of tungsten and bismuth which are lightweight, flexible, relatively inexpensive and more abundant compared to lead and non-toxic (Nikeghbal, et. al., 2020).

MATERIALS AND METHODS

Materials

The study utilized nano-powders of tungsten trioxide (WO_3), and bismuth oxide (Bi_2O_3) of 0.4 μm. The polyvinyl chloride (PVC) powder and dioctyl phthalate (DOP) oil were used as softeners to aid the flexibility of the radiation protective shields. A digital microbalance was used to obtain the weight of the precursor materials. Stainless steel was used for the construction of molds of 1.5 mm, 2 mm, and 2.5 mm of dimensions 15 cm x 15 cm each. A lead material of 2 mm thickness was used as a reference point.

The Cobra dosimeter was deployed to measure the baseline radiation from the X-ray machine before and during measurements using the constructed shields. X-ray machine unit of Toshiba product was used to characterize the constructed shields (Figure 1).

Figure 1: (a) X-ray Machine for Exposure and (b) Ionization chamber dosimeter (Cobra)

Molds Fabrication

The sample molds of dimensions 9.50 cm x 9.50 cm with varying thicknesses of 1.5, 2.0, and 2.5 ± 0.4 mm were fabricated with stainless steel to prevent stains that would contaminate the nano-polymer precursors as shown in Figure 2.

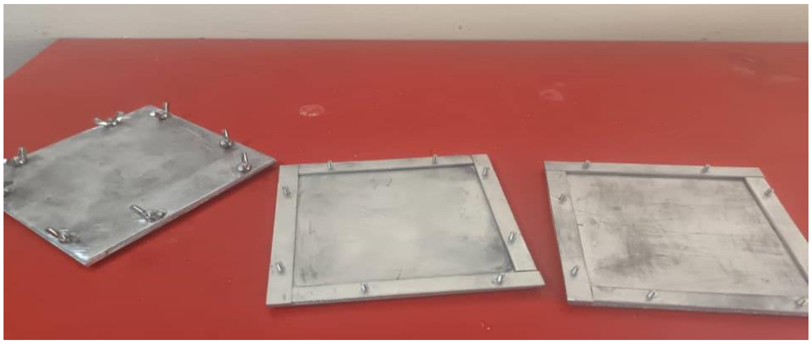

Figure 2: Fabricated of Stainless-Steel Molds

Preparation of the WO_3 and Bi_2O_3 Radiation Shields

To prepare tungsten and bismuth radiation shields, tungsten trioxide (WO_3) and Bismuth oxide (Bi_2O_3) nano-powders were used as the primary precursors; these were obtained from China. Emulsion PVC powder (also China) served as the polymer component, and DOP oil (China) as the softener as well as a lubricant. Epoxy oil (China) was used as a binder and a hardener was employed. All chemicals were of analytical grade and were used as purchased without further purification.

The proportionate weight of WO_3 and Bi_2O_3 was measured into two separate beakers containing given weights of DOP oil and thoroughly mixed using an ultrasonic mixer. Furthermore, PVC paste was made with DOP oil and dispersed for 15 min to obtain homogeneity, after which a proportion of epoxy was added for binding and integrity. Finally, the PVC paste was dissolved into the two beakers containing metallic oxides to form polymer composites with the metals. The resultant sample pastes (composites) were poured into the fabricated molds for a homogeneous thickness after sonication. The composite-filled molds were heated in an oven for 50 min at 180◦C and allowed to cool for 5 h (to room temperature). Two sets of flexible sample shields (W and Bi) were formed of thicknesses 1.5, 2.0, and 2.5 ± 0.4 mm. The synthesized flexible shields (Figure 4) were removed from the oven and preserved for characterization.

The proportional weights of the various precursors are provided in Table 1, while the synthesized W and Bi nanocomposite shields are shown in Figure 4.

Table 1: Percentage weights of precursors in W and Bi radiation shields

Wt% Metal Oxide nano Powder	wt% PVC	wt% DOP	Exopy Oil (15g)	
58.08 g WO_3	17 g	10 g	Resin 11.25 g	Hardener 3.75 g
58.08 g Bi_2O_3	17 g	10 g	11.25 g	3.75 g

Radiation Shielding

To measure X-ray shielding properties of the synthesized radiation shields, an X-ray unit (Toshiba, China) with a well-calibrated Cobra ionizing chamber dosimeter (made in China) was used. The intensities of X-ray radiation were measured with an average of 3 times without any absorbent shields giving (incident exposure) (I_o). The various shields as shown in Figure 4 were carefully placed on the ionization chamber as illustrated in Figure 3, and the passing intensities, shields exposure, I, were measured. After repeated measurements, the linear attenuation coefficient (μ) was calculated for each material using Equation (1) (Men'shchikov, 2016),

$$I = I_o e^{-\mu D} \quad (1)$$

Where I is the mean value of the X-ray intensity after passing through each shielding material, I_o is the intensity of the primary X-rays, D is the thickness of the shields, and μ is the linear attenuation coefficient.

The I_o can also be evaluated using Equation 2, based on the obtained X-ray machine data for KVp, mAs, dose, and dose rate. Given that the photon flux (I_o) is generally calculated by dividing the total energy per unit area (fluence) by the energy of a single photon, or by dividing the total number of photons by the area. The experimental result values of I and I_0 were obtained using Figure 3.

$$I_o = \frac{N\ (photons)}{A\ (cm^2)} \quad (2)$$

Where N is the total number of photons (KVp x mAs), and A is the area of the field size (Men'shchikov, 2016).

The mass attenuation coefficient (μ/ρ) of each sample shield was calculated by dividing linear attenuation coefficient by the density of the shielding materials.

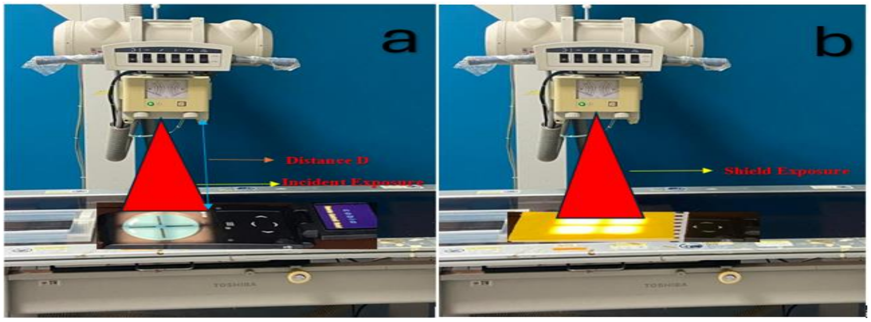

Figure 3: Experimental set-up for (a) incident I_o, and (b) shield I exposures

The half-value layer (HVL) was estimated from the thickness, volume, and weight (Table 2) of each sample; where HVL is the thickness of the protective material that attenuates the intensity of radiation by one-half as shown in Table 3. The HVL and relative efficiency were also evaluated using Equations 3 and 4, respectively:

$$HVL = 0.693/\mu \quad (3)$$

$$Relative\ efficiency = \frac{HVL_{nano-material} - HVL_{micro-material}}{HVL_{nano-material}} \times 100\% \quad (4)$$

The density of each mould was measured using the masses and volumes of the samples.

Figure 4: Fabricated Nano-Composite Shields

Table 2: Measured Parameters of the radiation shields

Materials (nanoparticles) weight (g)		Thickness (mm)	Squared Length (cm^2)	Vomue (cm^3)
Bismuth (Bi_2O_3)	Tungsten (WO_3)			
39.96	44.82	1.5	9.50 x 9.50	13.54
45.09	56.54	2.0	9.50 x 9.50	18.05
52.74	60.31	2.5	9.50 x 9.50	22.56

Table 4: Characteristics and X-ray shielding properties of the synthesized shielding materials at 40 KVp

Material	Thickness (mm)	ρ (g/cm^3)	D(m)	I_0 ($photons/cm^2$)	I_i (SD) ($photons/cm^2$)	I_i/I_0	μ (cm^{-1})	μ/ρ (cm^2/g)	Half Value Layer (cm)
Nano-Bi_2O_3	1.5	2.95	1.0	1.16	0.0	Undefined	Undefined	Undefined	Undefined
	2.0	2.50	1.0	1.16	0.0	Undefined	Undefined	Undefined	Undefined
	2.5	2.34	1.0	1.16	0.0	Undefined	Undefined	Undefined	Undefined
Nano-WO_3	1.5	3.31	1.0	1.16	0.0	Undefined	Undefined	Undefined	Undefined
	2.0	3.13	1.0	1.16	0.0	Undefined	Undefined	Undefined	Undefined
	2.5	2.67	1.0	1.16	0.0	Undefined	Undefined	Undefined	Undefined

Table 5: Characteristics and X-ray shielding properties of the synthesized shielding materials at 50 KVp

Material	Thickness(mm)	ρ (g/cm^3)	D(m)	I_0($photons/cm^2$)	I_i (SD) ($photons/cm^2$)	I_i/I_0	μ (cm^{-1})	μ/ρ (cm^2/g)	Half Value Layer (cm)
Nano-Bi_2O_3	1.5	2.95	1.0	2.29	0.0329	1.44×10^{-2}	4.24	1.44	0.16
	2.0	2.50	1.0	2.29	0.0203	8.86×10^{-3}	4.73	1.89	0.15
	2.5	2.34	1.0	2.29	0.0134	5.85×10^{-3}	5.14	2.20	0.13
Nano-WO_3	1.5	3.31	1.0	2.29	0.0518	2.26×10^{-2}	3.79	1.15	0.18
	2.0	3.13	1.0	2.29	0.0482	2.10×10^{-2}	3.86	1.23	0.18
	2.5	2.67	1.0	2.29	0.0168	7.34×10^{-3}	4.91	1.84	0.14

Table 6: Characteristics and X-ray shielding properties of the synthesized shielding materials at 60 KVp

Material	Thickness(mm)	ρ (g/cm^3)	D(m)	I_0($photons/cm^2$)	I_i (SD) ($photons/cm^2$)	I_i/I_0	μ (cm^{-1})	μ/ρ (cm^2/g)	Half Value Layer (cm)
Nano-Bi_2O_3	1.5	2.95	1.0	3.539	0.1127	3.19×10^{-2}	3.45	1.17	0.27
	2.0	2.50	1.0	3.539	0.0715	2.20×10^{-2}	3.90	1.56	0.18
2.5	2.34	1.0	3.539	0.06481	1.83×10^{-2}	4.00	1.71	0.17	
Nano-WO_3	1.5	3.31	1.0	3.539	0.2143	6.06×10^{-2}	2.80	0.84	0.25
	2.0	3.13	1.0	3.539	0.1669	4.71×10^{-2}	3.05	0.97	0.23

Material	Thickness(mm)	ρ (g/cm³)	D(m)	I_0(photons/cm²)	I_i (SD) (photons/cm²)	I_i/I_0	μ (cm⁻¹)	μ/ρ (cm²/g)	Half Value Layer (cm)
	2.5	2.67	1.0	3.539	0.08008	2.26 x 10^{-2}	3.79	1.42	0.18

The attenuation results showed that nano-particles of Bi demonstrated better shielding properties than that of W in radiation attenuation as recorded in Tables 3a, 3b and 3c.

RESULTS AND DISCUSSION

Crystal Structural Studies

X-ray diffraction (XRD) is a fundamental characterization technique used to determine the crystalline structure, phase composition, crystallite size, and lattice strain of nanoparticles (Bakri et al. 2024). For high-Z materials such as tungsten (WO_3) and bismuth (Bi_2O_3), XRD analysis provides critical insight into how structural features at the atomic scale influence radiation shielding performance (Bakri et al. 2024; Alawaideh et al. 2024). Although both materials are effective attenuators of ionizing radiation, their distinct crystallographic properties and phase behaviors produce notable differences in XRD patterns and their interpretation in shielding applications.

Figure 5 illustrates the XRD patterns of W and Bi, studied via PANalytical X'pert PRO high-resolution X-ray diffraction (HR-XRD) instrument with a CuKα (λ=0.15406nm) radiation source surface, in a 2θ range of 20° to 90°. A key distinction between tungsten and bismuth nanoparticles lies in their crystal structures and corresponding diffraction signatures (Alabsy& Abd Elzaher, 2023; Cullity& Stock, 2001). In Figure 5a, the tungsten sample is polycrystalline, with prominent diffraction peaks indexed to the body-centered cubic (BCC) structure of tungsten, corresponding to the JCPDS Card No. 46-1096, which are seen at 2θ values of 24.6°, 34.3°, 50.0° and 56.2° respectively in the (111), (200), (220) and (311) crystal planes. These peaks are generally sharp and intense, reflecting tungsten's high crystallinity and structural stability. In contrast, bismuth (Figure 5b) adopts a rhombohedral (A7-type) crystal structure, producing characteristic diffraction peaks of (111), (200), (321), (222), and (311) crystal planes, corresponding to 2θ values of 28.0°, 27.9°, 32.8°, 46.2°, 55.5°, and 74.5°, respectively, which are indexed to the JCPDS Card No. 27-0050 as depicted in Figure 5.

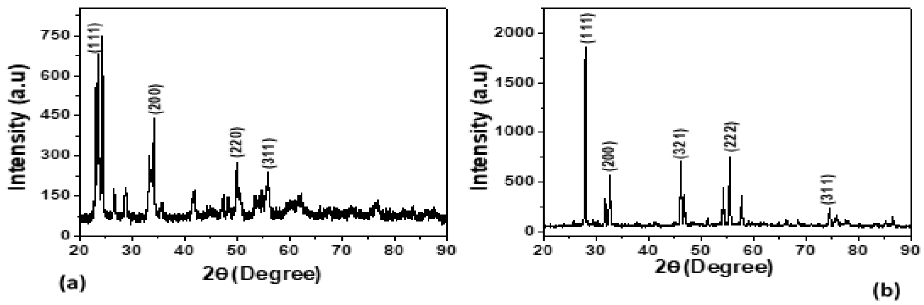

Figure 5: XRD patterns of radiation shields (a) tungsten, and (b) bismuth

The mean crystallite size estimated using the Scherrer equation, is a critical parameter derived from XRD peak broadening as shown in Equation (5) (Tyona et al. 2017).

$$D = \frac{K\lambda}{\beta Cos\theta} \quad (5)$$

where; D is the crystallite size, K is the shape factor (~0.9), λ is the X-ray wavelength, β is the peak broadening, and θ is the Bragg angle. The estimated crystallite size of bismuth nanoparticles in the most preferred growth plane (111) (Figure 5b) was 42 nm. This nanoscale refinement is advantageous for radiation shielding because it enhances surface area and improves dispersion within composite matrices (Elsafi et al. 2022; Kavaz et al. 2023). Whereas the estimated crystallite size of tungsten nanoparticles in the (111) crystal plane (Figure 5a) was 65 nm. Though, also nanoscale, tungsten nanoparticles display larger crystallite sizes or partial grain growth due to their high melting point and strong atomic bonding (Kavaz et al. 2023). Consequently, tungsten peaks appeared narrower, indicating larger coherent diffraction domains. While high crystallinity can improve mechanical stability, it may reduce the effectiveness of nanoscale dispersion (Kavaz et al. 2023), which is crucial for uniform attenuation.

Phase composition and oxidation behavior of materials is an important factor which can be studied with some information from the XRD patterns (Abou Hussein & Madbouly, 2024). Tungsten nanoparticles are prone to partial oxidation, leading to the formation of tungsten oxides such as WO_2 or WO_3 (Al-Saleh et al. 2023; Kavaz et al. 2023). These phases can be identified in the XRD patterns (Figure 5a) by the additional peaks at 26.7°, 28.8° and 41.8°, distinct from metallic tungsten. The presence of these oxide phases may alter shielding performance, since tungsten oxides have lower density and different electronic structures compared to pure tungsten (DeVanzo & Hayes, 2020; Kavaz et al. 2023). However, in some cases, mixed-phase systems can enhance scattering due to increased interfacial boundaries (Al-Saleh et al. 2023; Kavaz et al. 2023). Bismuth nanoparticles, similarly, may oxidize to form bismuth oxide (Bi_2O_3), which exists in multiple polymorphs (α, β, γ phases) (Tishkevich et al. 2024; Mohd Rau et al. 2024). XRD analysis is essential for distinguishing these phases, since each exhibit unique diffraction peaks. Bi_2O_3 phases are widely used in radiation shielding due to their stability and high attenuation coefficients (Tishkevich et al. 2024; Mohd Rau et al. 2024), and their identification via XRD is critical for correlating structure with performance.

Lattice strain and defects, inferred from peak broadening and shifts, further distinguish tungsten and bismuth systems. Bismuth nanoparticles often exhibit higher lattice strain due to their lower melting point and softer crystal structure, which can introduce defects and distortions (Tishkevich et al. 2024; Mohd Rau et al. 2024). These defects may enhance radiation interaction by increasing scattering sites. Tungsten, with its stronger metallic bonding and high thermal stability, typically shows lower lattice strain but fewer high-induced scattering centers (Mira et al. 2023). The balance between crystallinity and defect density is therefore crucial: high crystallinity ensures structural integrity; controlled defects can enhance attenuation efficiency (AbuAlRoos et al. 2020).

In terms of radiation shielding performance correlation, XRD-derived parameters such as crystallite size, phase purity, and lattice strain directly influence measurable quantities like the mass attenuation coefficient (μ/ρ) and half-value layer (HVL) (AbuAlRoos et al. 2020). For bismuth nanoparticles, smaller crystallite sizes and the presence of Bi_2O_3 phases often correlate with improved attenuation due to enhanced photon interaction probability and betterdispersion in composites. Tungsten nanoparticles can achieve high attenuation due to their density (AbuAlRoos et al., 2020), but XRD evidence of oxidation or large crystallite size as observed earlier, may indicate reduced effectiveness in nanocomposite systems. This collaborates the results of Mohd Rau et al. 2024 and Sayyed et al. 2021. Therefore, XRD serves not only as a structural characterization tool but also as a predictive indicator of shielding behavior.

Morphological Studies

The morphology of high-Z nanoparticles such as tungsten and bismuth play a decisive role in determining their radiation shielding efficiency, particularly when embedded in composite systems. Although both materials are effective attenuators of X-rays and γ-rays, their nanoscale structural characteristics such as particle size, shape, dispersion, and interfacial behavior, lead to markedly different shielding outcomes.

Figure 6 depicts the field emission scanning electron micrographs (FESEM) of tungsten (W) and bismuth (Bi) nanoparticles studied with a FEI Nova NanoSEM450 field emission scanning electron microscope. A primary morphological distinction between the two materials lies in particle size distribution and its effect on attenuation. The FESEM micrographs, Figure (6b) illustrates that the bismuth nanoparticles were typically synthesized in smaller and more uniform grain sizes range (≈5–50 nm), enabling improved homogeneity within host matrices. This fine dispersion enhances photon–matter interaction probability by reducing interparticle spacing and minimizing voids (Al-Saleh et al. 2023; Kavaz et al., 2023). In contrast, the tungsten nanoparticles (Figure 6a), exhibit typical grain sizes in the range 10–100 nm, with large clusters, which may be adduced to their higher density and surface energy (Mohamed et al. 2025). While tungsten's intrinsic density (19.3 g/cm³) theoretically favors attenuation, the formation of aggregates reduces effective surface area and creates heterogeneities that can compromise shielding performance (Mohamed et al., 2025). Studies have shown that nanoscale Bi particles perform better than their microscale counterparts and, in some composite systems, rival or exceed tungsten-based fillers when dispersion is optimized (Elsafi et al., 2022; Kavaz et al., 2023).

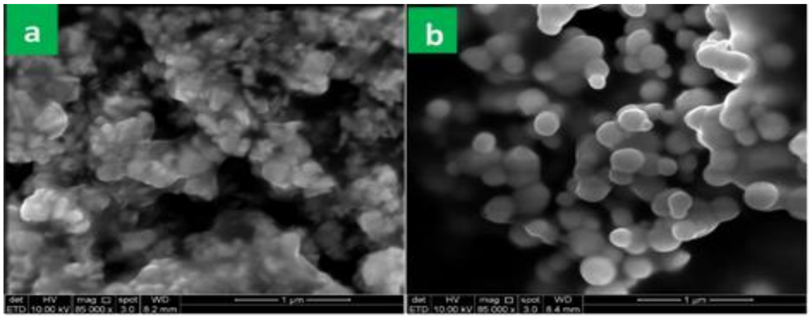

Figure 6: Field emission scanning electron micrographs of radiation shields (a) tungsten, and (b) bismuth

Geometric morphology (particle shape) further differentiates the two systems (Bi_2O_3 and WO_3). Bismuth nanoparticles are readily synthesized in diverse morphologies, including spherical particles, nanosheets, and hierarchical structures such as nanoflowers. Spherical Bi nanoparticles are particularly advantageous for radiation shielding due to their isotropic geometry, which ensures uniform attenuation regardless of photon incidence direction (Mohamed et al., 2025; Elsafi et al., 2022; Kavaz et al., 2023), as it is readily the case withFigure (6b). Tungsten nanoparticles, on the other hand, are commonly obtained as spherical particles, nanorods, or nanowires, as well as in oxide forms (e.g., WO_3 nanosheets). While one-dimensional structures such as nanorods can enhance mechanical reinforcement in composites, they often introduce anisotropy in shielding performance and are less efficient in packing compared to spherical particles. Consequently, bismuth exhibits greater morphological versatility and adaptability for optimizing attenuation (Singh et al., 2019; Kerli et al., 2026).

A critical factor linking morphology to radiation shielding performance is dispersion within the matrix. Bismuth nanoparticles generally demonstrate superior compatibility with polymer matrices such as poly (methyl methacrylate) (PMMA) and polyvinyl chloride (PVC), leading to uniform spatial distribution. This homogeneous dispersion minimizes radiation leakage pathways and ensures consistent attenuation throughout the material. Tungsten nanoparticles, by contrast, are more prone to agglomeration due to strong interparticle interactions (Figure 6a). Without appropriate surface modification or functionalization, tungsten fillers tend to form clusters that introduce porosity and reduce effective shielding efficiency as demonstrated in Figure 6a. This difference highlights a key practical advantage of bismuth: its ability to maintain nanoscale dispersion at relatively high loading fractions.

Another important morphological consideration is packing density and porosity. Effective radiation shielding requires minimizing void spaces within the material. Bismuth nanoparticles, due to their smaller size and better dispersion, can fill interstitial gaps more effectively, leading to higher packing uniformity (Zhang et al., 2020; Kerli et al., 2026). Tungsten nanoparticles, despite their higher intrinsic density, may exhibit lower effective density in composites if agglomeration leads to uneven distribution. Consequently, the theoretical advantage of tungsten's density is not always fully realized in practical systems. Optimized bismuth nanoparticle systems often achieve comparable or superior attenuation by maximizing packing efficiency and reducing porosity (Singh et al., 2019; Zhang et al., 2020), which clearly collaborates our current results.

The relationship between morphology and shielding performance is evident in experimentally measured parameters such as the mass attenuation coefficient (μ/ρ) and half-value layer (HVL) (Singh et al., 2019; Zhang et al., 2020; Kerli et al., 2026). Uniformly dispersed, nanoscale bismuth particles consistently yield lower HVL values, indicating better shielding efficiency at reduced thicknesses. This collaborates our earlier result in Figure (5b) and Table (2). Tungsten nanoparticles can achieve high attenuation coefficients when dispersion is carefully controlled; however, performance variability is more pronounced due to morphological challenges (Bashter, 1997; Kerli et al., 2026). This underscores the importance of nanoscale engineering in achieving reliable and reproducible shielding properties.

Despite these advantages, both materials present trade-offs. Bismuth's lower density relative to tungsten limits its effectiveness at very high photon energies, where density becomes a dominant factor (Cullity& Stock, 2001). Conversely, tungsten's morphological limitations, particularly agglomeration and processing difficulty, pose challenges for large-scale application (Mohamedet al., 2025; Elsafi et al., 2022; Kavaz et al., 2023). These complementary strengths and weaknesses have led to increasing interest in hybrid nanocomposites, where bismuth and tungsten nanoparticles are combined to exploit the high dispersion of Bi and the high density of W.

Radiation Shielding

The study has investigated the X-ray attenuation properties of the two nano-structured radiation shields with thicknesses: 1.5, 2.0 and 2.5 mm against X-ray exposure. The resultsdemonstrated half values layers (HVL) for WO_3, and Bi_2O_3 at different exposures of 40, 50 and 60 KVp with total shielding at the 40 KVp for all the nano shields at all the thicknesses. This agrees with the research results of Nikeghbal, et.al (2020), which stated that, the nano-structured samples are so effective in the attenuation of X-rays at lower energies. For the higher X-ray exposures at 50 KVp, the Bi_2O_3 shield demonstrated HVLs of 0.16, 0.16, and 0.13cm forshields thicknesses of 1.5, 2.0, and 2.5 mm respectively, whereas the WO_3, shields showed HVLs of 0.18, 0.18, and 0.14 for the same thicknesses. This is an indication that the Bi_2O_3 nanostructured radiation shields offer ahigher radiation shielding ability ascompared to its W counterpart, which well collaborates the earlier results XRD and FESEM even though both materials exhibit good attenuation of the radiation beams from the X-ray machine. This is a clear demonstration that WO_3 and Bi_2O_3 nanoparticles have promising potentials to replace lead as radiation shielding material.

At the 60 KVp X-ray exposures of both materials were still able to significantly attenuate the radiation beam showing half values layers of 0.27, 0.18 and 0.17 mm for the various thicknesses of the Bi_2O_3 nano shields whereas, HLVs of 0.25, 0.23, and 0.18 mm were recorded for the same thicknesses of W nano shields this is comparable to the Half-Value Layer (HVL) of lead at 60 kVp is approximately 0.12 to 0.13 mm of leadas reported by Tochaikul et.al.(2025). Furthermore, the linear attenuation coefficients (μ) for Bi and W were estimated using Equation 1, and as shown in Tables 3b and 3c. This isalso a demonstration of the shielding capability of Bi_2O_3 nano particles over the WO_3. The exposure at 60 KVp as produces a similar effect with the μ of 3.42, 3.90, and 4.00 cm^{-1} for Bi_2O_3 and 2.80, 3.05 and 3.79 cm_{-1} for WO_3 considering the above-mentioned precursors shields thicknesses respectively as shown in Tables 2 and 3. This effectiveness demonstrated the polymer fillers' ability to be used as shield materials to adequately attenuate the X-ray beams at lower energies. This agrees with Azman, et. al (2013) that filler-reinforced polymers have gained increasing attention from X-ray technologists in radiation shielding since polymers have great potential in many important applications by virtue of their unique properties, such as low density, the ability to form intricate shapes, optical transparency, low manufacturing cost and toughness.

Moreover, nano-sized Bi_2O_3 composites consist of higher density compared to the nano-sized composites therefore, the distribution of the nano-sized Bi_2O_3 in the resin should also be different from that presented by the nano-sized micro WO_3, thus resulting in a more uniform dispersion in the resin and fortified prototype mold. Consequently, the chances of an X-ray photon with lower energy to interact and be absorbed by Bi_2O_3 particles may be higher in nano-sized Bi_2O_3 than that of theWO3-epoxy composites. As the photon energy increases, the photon (X-ray) penetration through the material without absorption interaction increases since less photoelectric effect relative to the Compton Effect predominates. Thus, the X-ray attenuation by the absorbing material decreases since the Compton interaction is weakly dependent on Z and E and this interaction only takes place between the incident photon and one of the outer shell electrons of an atom in the absorbing material. Therefore, our findings agree with the result of Azman, et.al. (2013) on micro-sized and nano-sized tungsten oxide-epoxy composites for radiation shielding of diagnostic X-rays. The findings indicate that nano-structured samples are more effective in the attenuation of X-rays at lower energies and with less weight and are harmless compared to lead.

CONCLUSION

The fabrication and characterization of tungsten- and bismuth-based X-ray radiation shields demonstrated that both materials possess significant potential for effective X-ray attenuation while offering alternatives to conventional lead shielding. X-ray diffraction (XRD) analysis confirmed the successful formation and preservation of the crystalline phases of tungsten and bismuth after fabrication. Scanning electron microscopy (SEM) revealed a relatively homogeneous microstructure with good particle distribution and limited porosity, indicating that the fabrication process produced dense composites favorable for minimizing radiation transmission. The combined structural and morphological characterization established a strong correlation between material quality and radiation shielding efficiency. Experimental evaluation of the X-ray attenuation coefficient showed that attenuation increased with material density and atomic number, with bismuth-based shields exhibiting slightly superior shielding performance over tungsten-based shields. The estimated HVL values were consistent with the measured linear attenuation coefficients. Overall, the results demonstrate that both fabricated materials are suitable candidates for diagnostic X-ray shielding applications, with bismuth offering better attenuation efficiency. These findings provide a foundation for further development of advanced, lead-free radiation shielding materials and support further optimization of fabrication parameters to enhance microstructural uniformity and shielding performance.

REFERENCES

Fahrul Bakri, Paulus Lobo Gareso, Dahlang Tahir, Advancing radiation shielding: A review the role of Bismuth in X-ray protection; *Rad. Phys. Chem.*217 (2024)111510

Samer E'layanAlawaideh, M.I. Sayyed, K.A. Mahmoud, M. Hanfi, Mohammad A. Imheidat, Kawa M. Kaky, Hammam Abdurabu Thabit, Mohamed Elsafi, Effect of different metal oxides on the Radiation shielding features of borate glasses; Rad. Phys. Chem. 220 (2024) 111720

Amit Kumar, Amit Kumar, Cabral-Pinto M.M.S. , Ashish K. Chaturvedi , Aftab A. Shabnam , Gangavarapu Subrahmanyam , Raju Mondal, Dipak Kumar Gupta , Sandeep K. Malyan, Smita S. Kumar, Shakeel A. Khan and Krishna K. Yadav; Lead Toxicity: Health Hazards, Influence on Food Chain, and Sustainable Remediation Approaches; International Journal of Environmental Research and Public Health. 17 (2020) 2179.

Mahmoud T. Alabsy and Mohamed Abd Elzaher; Radiation shielding performance of metal oxides/EPDM rubber composites using Geant4 simulation and computational study; *Scientific Reports* (2023) 13:7744

E. M. Abou Hussein, A. M. Madbouly; Chemical and radiation shielding effectiveness of some heavy metal oxide glasses for immobilizing radioactive wastes; J.Austra.Cera. Soc. (2024) 60:127–142

Wafa M. Al-Saleh, Haifa M. Almutairi, M. I. Sayyed, & Mohamed Elsaf; Multilayer radiation shielding system with advanced composites containing heavy metal oxide nanoparticles: a free-lead solution; *Scientific Reports* (2023) 13:18429

Michael DeVanzo, Robert B. Hayes; Ionizing radiation shielding properties of metal oxide impregnated conformal coatings; *Rad. Phys. Chem.* 171 (2020) 108685

Daria I. Tishkevich, Stepan A. German, Anastasia A. Rotkovich, Tatiana N. Vershinina, Aliaksandr L. Zhaludkevich, Yuan Yao, Maksim V. Silibin, Ihar U. Razanau, Tatiana I. Zubar, Anastasia A. Bondaruk, M.I. Sayyed, Alex V. Trukhanov; Isostatic hot-pressed tungsten radiation shields against gamma radiation; *J. Mater. Res. Technol.* 30 (2024) 4347–4352

AiniAyunniMohd Rau, Raihana Bahru, Siti Nur AshakirinMohdNashruddin, JumrilYunas; Advances of nanostructured metal oxide as photoanode in photoelectrochemical (PEC) water splitting application, *Heliyon* 10 (2024) e39079

Men'shchikov, A. (2016). Uncertainties and biases of source masses derived from fits of integrated fluxes or image intensities. *Astronomy & Astrophysics*, *593*, A71.

Gemanam, S. J., Nursakinah Suardi, Barnabas A. Ikyo, Samson Damilola Oluwafemia, Terver Daniel, Samuel T. Kungur, (2020). Biostimulation effects as a result of temperature variation in stimulated diabetic blood based on specific absorption rate (SAR) in laser therapy, *Journal of the Nigerian Society of Physical Sciences*,**3**(2021), pp. 66–73

MiraNatasha Azman, NadinJamal Abualroos, Khatijah,Aisha Yaacob, Rafidah Zainon;Feasibility of nanomaterial tungsten carbide as lead-free nanomaterial-based radiation shielding; *Rad. Phys. Chem.* 202 (2023) 110492

Nadin Jamal AbuAlRoos, MiraNatasha Azman, Noorfatin Aida Baharul Amin, Rafidah Zainon; Tungsten-based material as promising new lead-free gamma radiation shielding material in nuclear medicine; *PhysicaMedica* 78 (2020) 48-57

Elsafi M., El-Nahal M. A., Sayyed M. I., Saleh I. H. and Abbas M. I.; Novel 3-D printed radiation shielding materials embedded with bulk and nanoparticles of bismuth. *Scientific Reports*, 12 (2022), 12467 1 - 10.

Kavaz, E., et al. (2023). Bismuth-based nanomaterials for radiation shielding applications: A review. *Radiation Physics and Chemistry*, 203, 110567.

Mohamed Elsafi, Mohamed Abdellatief, Aljawhara H. Almuqrin, Shoaa M. Al-Balawi and M.I. Sayyed (2025). Enhanced Gamma-ray Shielding With Nanostructured PbO, Bi2O3, and WO3 Composites. Journal of Nanoparticle Research, 27, 257.

Tochaikul, Gunjanaporn, et al. "Enhancing radiation shielding capabilities with epoxy-resin composites reinforced with coral-derived calcium carbonate fillers." *Polymers* 17.1 (2025): 113.

Süleyman Kerli, Yusuf Kavun, Handan Özlü Torun, &M. Enes Balkan; Structural characterization and evaluation of radiation-shielding performances of layered and composite ZnO–CdO thin films; J Mater Sci: Mater Electron (2026) 37:863

Zhang, H., et al. (2020). Synthesis and characterization of tungsten nanoparticles for shielding applications. *J. Mater. Sci.: Materials in Electronics*, 31, 14567–14575.

Bashter, I. I. (1997). Calculation of radiation attenuation coefficients. *Annals of Nuclear Energy*, 24, 1389–1401.

Cullity, B. D., & Stock, S. R. (2001). *Elements of X-ray Diffraction* (3rd ed.). Prentice Hall.